2013 IEEE International Conference on Robotics and Automation (ICRA)
Karlsruhe, Germany, May 6-10, 2013

Experimental Design Verification of a Compliant Shoulder Exoskeleton

Kai Xu*, *Member, IEEE* and Dong Qiu, *Student Member, IEEE*

***Abstract*—Many existing exoskeletons have followed a similar design approach: a rigid kinematic chain is actuated to mobilize a human wearer. However, in a clinical setting for rehabilitation where one exoskeleton is shared by multiple patients, it will be difficult to guarantee on-site adjustments can make the rigid exoskeleton fit each patient kinematically perfectly. This paper proposed an alternative exoskeleton design that uses compliant continuum mechanisms. Its intrinsic flexibility adapts to different human anatomy automatically. Design concepts and component descriptions were elaborated for this shoulder exoskeleton, including kinematics, construction, actuation, transmission schemes, etc. A series of experiments were conducted to characterize shapes of the flexible members within the continuum structure as well as demonstrate the effectiveness of using such an exoskeleton to assist different patients with their limb motions.**

I. Introduction

EXOSKELETON research attracted a lot of attentions in the past decades. Numerous exoskeleton systems were developed for upper and lower limbs for military and medical purposes (e.g. [1, 2]). These exoskeleton systems either aim at augmenting a healthy wearer's physical capabilities with robotic actuation or to allow rehabilitation for neuromuscular defects after stroke or injury. Examples include the Mihailo Pupin Institute exoskeleton for paraplegics rehabilitation [3] from the 70s and many recent advances, such as the performance-augmenting exoskeleton from UC Berkeley [4], the load-carrying exoskeleton from MIT [5], rehabilitation exoskeletons for lower limbs [6-10], and those for upper limbs [11-18]. Actuation schemes of the aforementioned systems include hydraulic [4] or pneumatic cylinders [3, 6, 16], pneumatic muscle actuators [11], cable actuations [8, 12, 18], parallel mechanisms [9, 13, 15], gearmotors [19], etc.

Besides these exoskeleton systems, research was also about enabling technologies, such as inertia compensation [20], sensing & control [5, 21-24], ergonomics [25-27], new actuators [28, 29], etc.

Many existing exoskeleton systems followed one similar design approach: using different control and sensing schemes, rigid kinematic chains are actuated to mobilize an attached human wearer. The use of rigid links in an exoskeleton might be justified in applications for strength augmentation to undertake excessive external loads and shield the wearer. But the use of rigid links introduced drawbacks such as bulkiness, high inertia, and most importantly the difficulty of maintaining kinematic compatibility between exoskeleton and human anatomy. In a clinical setting for rehabilitation where one exoskeleton consisting of rigid links is shared by multiple patients, it is even more difficult to guarantee the on-site adjustments performed by therapists can make the rigid exoskeleton fit each individual patient perfectly. Hence design approaches of using non-rigid components could be explored. These attempts include a simulation to show the possibility of using elastic cords to assist walking [30], an upper body exoskeleton using home-made pneumatic artificial muscles [31], a cable-driven upper-limb exoskeleton [17, 18], and the continuum shoulder exoskeleton presented in this paper and shown in Fig. 1 (A preliminary version of this design with an underperformed hence abandoned actuation unit was presented in [32]).

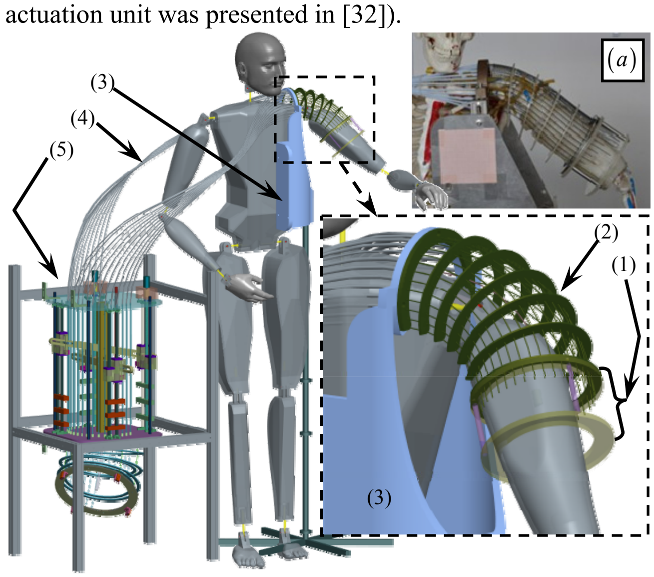

Fig. 1. The compliant continuum shoulder exoskeleton: (1) an upper arm sleeve, (2) a flexible continuum joint brace, (3) a body vest, (4) a set of guiding cannulae, and (5) an actuation unit. The actual system is pictured in inset (a) and Fig. 6.

This paper presents design concepts, kinematics, actuation, transmission scheme, shape identification, and manikin trials of the continuum shoulder exoskeleton as shown in Fig. 1. Major contribution of this paper is the proposal and its experimental validation of designing compliant continuum exoskeletons for rehabilitation. Intrinsic compliance of such a continuum exoskeleton adapts to different human anatomy automatically and can always assure the kinematic

Manuscript received Sept 17*th*, 2012. This work was supported in part by the National Program on Key Basic Research Projects (the 973 Program) #2011CB013300, and in part by Program for New Century Excellent Talents in University (the NCET Program).

Both authors are with the RII Lab (Lab of Robotics Innovation and Intervention), UM-SJTU Joint Institute, Shanghai Jiao Tong University, Shanghai, 200240, China (asterisk indicates the corresponding author, phone: 86-21-34207220; fax: 86-21-34206525; emails: k.xu@sjtu.edu.cn and d.qiu@sjtu.edu.cn)

compatibility between itself and a group of patients. Minor contributions of this paper include the design of an actuation unit with a continuum transmission to push and pull flexible members in the design in a synchronized manner.

The paper is organized as follows. Section II presents the design concept and the system overview. Section III presents nomenclature and kinematics so that the system description presented in Section IV can be better elaborated. Section V presents experimental validation, characterization, and manikin trials of the continuum exoskeleton to demonstrate the effectiveness of using one exoskeleton to adapt to multiple patients. Conclusions and future work are summarized in Section VI.

II. Design Concept

The continuum shoulder exoskeleton design shown in Fig. 1 consists of a rigid upper arm sleeve (#1), a flexible continuum joint brace (#2), a body vest (#3), a set of guiding cannulae (#4), and an actuation unit (#5). Actuation of the flexible joint brace (#2) orients a patient's upper arm. This work is inspired by [33, 34] where downscaled such continuum structures were used in surgical robots.

Structure of the continuum brace (Fig. 1.#2) is also depicted in Fig. 2. It consists of an end ring, a base ring, a few spacer rings and several secondary backbones. All the backbones are made from thin NiTi (Nickel-Titanium alloy) rods. The secondary backbones are only attached to the end ring and can slide in holes of the spacer rings and the base ring. Backbones are routed through a set of guiding cannulae (Fig. 1.#4) to the actuation unit (Fig. 1.#5), which pulls and pushes these secondary backbones simultaneously to achieve a bending to orient a patient's upper arm. Miniature springs are used to keep the spacer rings evenly distributed to prevent buckling of the secondary backbones.

The flexible continuum shoulder brace (Fig. 1.#2) has 2 DoFs (Degrees of Freedom) because it can only orient an upper arm (also referring to Fig. 4). Referring to Fig. 2, an imaginary centrally-located primary backbone characterizes length and shape of the continuum brace. The actual shape of the continuum brace depends on a minimum of the potential energy distributed along the backbones with constraints from the wearer's anatomy.

Since a human shoulder joint can be approximated by a 3-DoF spherical joint, a rotation along the axis of the upper arm is not assisted by the current design. The upper arm can rotate freely with respect to the upper arm sleeve. To be noted, in Fig. 4 three serially connected revolute joints were used to representing a spherical joint since an off-the-shelf spherical joint doesn't have a motion range big enough to demonstrate the motion capability of this shoulder exoskeleton.

Advantages of this structure include: i) comfort and safety introduced by the inherent compliance of this continuum structure, ii) passive adaptation to different anatomical geometry, iii) size scalability, iv) actuation redundancy introduced by using multiple secondary backbones to drive a 2-DoF bending that loads on backbones can be redistributed and buckling risks can be minimized, and v) design compactness achieved by dual roles of these secondary backbones as both structural components and motion output members.

III. Nomenclature and Kinematics

The nomenclature and the kinematics assume that the continuum brace bends in a planar manner within the bending plane as shown in Fig. 2. Shapes of the secondary backbones are assumed by a sweeping motion of the structure's cross section along the primary backbone. The cross section is assumed rigid and perpendicular to the primary backbone. Different from previously published results [33-35], this work doesn't assume shape of the imaginary primary backbone to be circular, which will be verified by the experiments.

A. Nomenclature

Nomenclatures are defined in Table I, while coordinate systems of the continuum brace are defined as below:

- *Base Ring Coordinate System* (BRS) is designated as $\{b\} \equiv \{\hat{\mathbf{x}}_b, \hat{\mathbf{y}}_b, \hat{\mathbf{z}}_b\}$. It is attached to the base ring of the continuum brace, whose XY plane coincides with the base ring and its origin is at the center of the base disk. $\hat{\mathbf{x}}_b$ points from the center of the base disk to the first secondary backbone while $\hat{\mathbf{z}}_b$ is perpendicular to the base ring. Secondary backbones are numbered according to the definition of δ_i.
- *Bending Plane Coordinate System 1* (BPS1) is designated as $\{1\} \equiv \{\hat{\mathbf{x}}_1, \hat{\mathbf{y}}_1, \hat{\mathbf{z}}_1\}$ which shares its origin with $\{b\}$ and has the continuum brace bending in its XZ plane.
- *Bending Plane Coordinate System 2* (BPS2) is designated as $\{2\} \equiv \{\hat{\mathbf{x}}_2, \hat{\mathbf{y}}_2, \hat{\mathbf{z}}_2\}$ obtained from $\{1\}$ by a rotation about $\hat{\mathbf{y}}_1$ such that $\hat{\mathbf{z}}_1$ becomes backbone tangent at the end ring. Origin of $\{2\}$ is at center of the end ring.
- *End Ring Coordinate System* (ERS) $\{e\} \equiv \{\hat{\mathbf{x}}_e, \hat{\mathbf{y}}_e, \hat{\mathbf{z}}_e\}$ is fixed to the end ring. $\hat{\mathbf{x}}_e$ points from center of the end ring to the 1*st* secondary backbone and $\hat{\mathbf{z}}_e$ is normal to the end ring. $\{e\}$ is obtained from $\{2\}$ by a rotation about $\hat{\mathbf{z}}_2$.

TABLE I
Nomenclature Used in This Paper

m	Number of the secondary backbones
i	Index of the secondary backbones, $i = 1,2,\cdots,m$
r_i	Distance from the imaginary primary backbone to the i*th* secondary backbone. r_i can be different for different i.
β_i	β_i characterizes the division angle from the i*th* secondary backbone to the 1*st* secondary backbone. $\beta_1 \equiv 0$ and β_i remain constant once the brace is built.
L, L_i	Lengths of the imaginary primary and the i*th* secondary backbones measured from the base ring to the end ring.
d_i	Diameter of the i*th* secondary backbone
$\rho(s), \rho_i(s_i)$	Radius of curvature of the primary and the i*th* secondary backbones.
$\mathbf{q}$	$\mathbf{q} = [q_1 \ q_2 \ \cdots \ q_m]^T$ is the actuation lengths for the

	secondary backbones and $q_i \equiv L_i - L$.
$\theta(s)$	The angle of the tangent to the imaginary primary backbone in the bending plane. $\theta(L)$ and $\theta(0)$ are designated by θ_L and θ_0, respectively. $\theta_0 = \pi/2$.
δ_i	A right-handed rotation angle about $\hat{\mathbf{z}}_1$ from $\hat{\mathbf{x}}_1$ to a ray passing through the imaginary primary backbone and the i*th* secondary backbone.
δ	$\delta \equiv \delta_1$ and $\delta_i = \delta + \beta_i$.
$\boldsymbol{\psi}$	$\boldsymbol{\psi} \equiv [\theta_L \ \ \delta]^T$ defines the configuration of the brace.
${}^b\mathbf{p}(s)$	Position vector of a point along the primary backbone in $\{b\}$. ${}^b\mathbf{p}(L)$ is the tip position and is designated by ${}^b\mathbf{p}_L$.

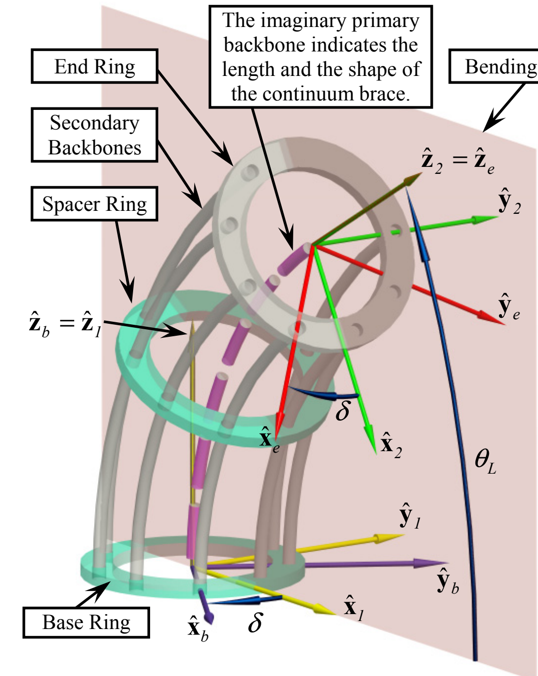

Fig. 2. Nomenclature and coordinates of the continuum brace

B. Kinematics

Thorough kinematics analysis of such a continuum brace can be found in [34-38]. This work here emphasizes the shape of the primary backbone to be non-circular (the result also applies if the shape is circular). This work also extends the modeling for arbitrary arrangements of the secondary backbones by assigning different values to r_i and β_i.

Configuration of the continuum brace is parameterized by $\boldsymbol{\psi} = [\theta_L \ \ \delta]^T$. Since shapes of the secondary backbones are assumed by a sweeping motion of the structure's cross section along the primary backbone, projection of the i*th* secondary backbone on the bending plane is a curve which is offset by Δ_i from the primary backbone. Its radius of curvature and arc-length are indicated by $\rho_i(s_i)$ and s_i. They are related to the parameters of the primary backbone as follows:

$$\rho(s) = \rho_i(s_i) + \Delta_i \tag{1}$$

Where $\Delta_i \equiv r_i \cos\delta_i$.

The length of the primary backbone and the length of the i*th* backbone are related according to:

$$L_i = \int ds_i = \int (ds_i - ds + ds) = L + \int (ds_i - ds) \tag{2}$$

Referring to Fig. 3, the integral above can be rewritten as in Eq. (3). Substituting Eq. (1) into Eq. (3) gives Eq.(4), which leads to the result as in Eq. (5):

$$\int (ds_i - ds) = \int_0^{\theta_0-\theta_L} (\rho_i(s_i) - \rho(s))\, d\theta \tag{3}$$

$$\int_0^{\theta_0-\theta_L} (\rho_i(s_i) - \rho(s))\, d\theta = -\int_0^{\theta_0-\theta_L} \Delta_i d\theta \tag{4}$$

$$L_i = L - r_i\cos\delta_i(\theta_0 - \theta_L) = L + r_i\cos\delta_i(\theta_L - \theta_0) \tag{5}$$

Referring to the definition of q_i in Table I, Eq. (5) gives:

$$q_i = r_i\cos\delta_i(\theta_L - \theta_0),\ i = 1, 2, \cdots, m \tag{6}$$

Eq. (6) states that actuation of this continuum brace only depends on the values of θ_L and δ, no matter what the actual shape of the primary backbone is. This characteristics provides a particular advantage: when the brace is put on different patients, different anatomies give different shapes of the primary backbone, but the actuation remains the same while orienting the limb to the same direction (the direction is characterized by θ_L and δ).

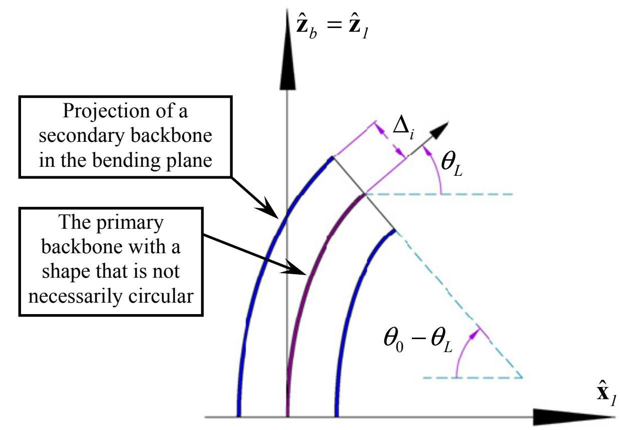

Fig. 3. The primary backbone and the projection of secondary backbones in the bending plane

Rotation matrix ${}^b\mathbf{R}_e$ associates $\{e\}$ and $\{b\}$:

$${}^b\mathbf{R}_e = \mathrm{R}(\hat{\mathbf{z}}_b, -\delta)\mathrm{R}(\hat{\mathbf{y}}_1, \theta_0 - \theta_L)\mathrm{R}(\hat{\mathbf{z}}_2, \delta) \tag{7}$$

Where $\mathrm{R}(\hat{\mathbf{n}}, \gamma)$ designates rotation about $\hat{\mathbf{n}}$ by an angle γ.

Tip position of the continuum brace is given by:

$${}^b\mathbf{p}_L = {}^b\mathbf{R}_1 \left[\int_0^L \cos(\theta(s))\, ds \quad 0 \quad \int_0^L \sin(\theta(s))\, ds \right]^T \tag{8}$$

Where ${}^b\mathbf{R}_1 = \mathrm{R}(\hat{\mathbf{z}}_b, -\delta)$ and the integrals depend on the actual shape of the primary backbone.

IV. System Descriptions

System components of this shoulder exoskeleton mainly include the continuum brace and the actuation unit. Simultaneous actuation of the secondary backbones in the continuum brace orients the wearer's upper arm.

A. The continuum brace

Main design parameters of the continuum brace include length of the imaginary primary backbone (L), size and placement of the secondary backbones (d_i , r_i and β_i).

As detailed in [32], length of the imaginary primary backbone (L) is determined to be 220mm and all the r_i are set to be 60mm so that the exoskeleton is big enough to fit a reasonable group of patients. The continuum exoskeleton supposes to provide enough assistance to patients for their ADLs (Activities of Daily Living). According to [39], a shoulder joint provides a torque as high as 10 Nm to drive the upper limb. A preliminary statics model presented in [32] suggested that the use of 25 secondary backbones at diameters of 1.2mm leaded to a maximal stress in the NiTi material well below the allowed value. Hence 25 secondary backbones will be used. As shown in Fig. 4, the backbone arrangement corresponds to the indicated β_i values. The use of more secondary backbones can reduce the backbones' diameter and it brings a few additional advantages: i) thinner backbones increase the flexibility of the exoskeleton hence leads to a potential increase in user comfort; ii) failure of one thin backbone would not fail the entire exoskeleton hence reliability and safety can be potentially increased.

Main design parameters are summarized in Table II.

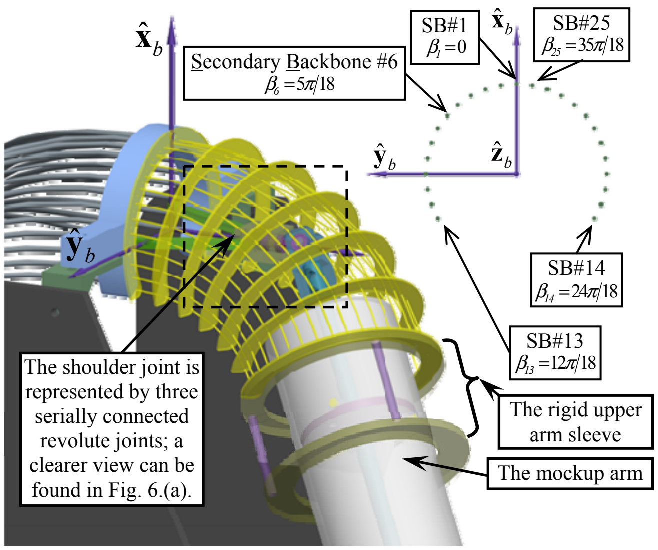

Fig. 4. The continuum brace with the arrangement of the secondary backbones (part of the brace is hidden for better visualization of the joint)

TABLE II

DESIGN PARAMETERS OF THE CONTINUUM BRACE

$L = 220mm$	$d_i = 1.2mm$	$r_i = 60mm$
$\beta_1 = 0, \beta_2 = \pi/18, \beta_3 = 2\pi/18, \cdots, \beta_{13} = 12\pi/18$		
$\beta_{14} = 24\pi/18, \beta_{15} = 25\pi/18, \cdots, \beta_{25} = 35\pi/18$		

B. The actuation unit and the transmission

Actuation of the continuum brace involves simultaneous pushing and pulling of 25 secondary backbones. However, as explained in Section III.B, the continuum brace only possesses 2 DoFs to orient a wearer's upper arm. Hence, an important aspect of the actuation unit is to design a transmission system which maps two inputs to 25 outputs according to the kinematics in Eq. (6).

The attempt of designing such a transmission using hydraulic cylinders was detailed in [32]. However that design encountered severe leaking problems and abandoned.

A completely redesigned actuation unit is shown in Fig. 5. It has a continuum transmission which consists of two layers of the continuum structure shown in Fig. 2:

- The inner layer has 25 secondary backbones which are routed to form the shoulder brace through the set of guiding cannulae. Arrangement of these backbones is identical to the brace except that diameter of this layer is twice of the shoulder brace. According to the kinematics in Eq. (6), bending of the inner layer will bend the shoulder brace for a double amount.
- The outer layer has 4 secondary backbones that are placed 90º away from each other. Bending of this outer layer bends the inner layer to the same orientation since end rings of the inner and the outer layers are rigidly attached.

Motorized ball screws push and pull backbones of the outer layer of the continuum transmission. Levers inverse the push-pull motions for backbones with a division angle of 180º. A few sliding blocks prevent bulking of these backbones.

This actuation unit design is based on an assumption that the inner layer is bent into a shape similar to that of the outer layer. Experimental results shown in Fig. 9 and Fig. 10 will validate this assumption.

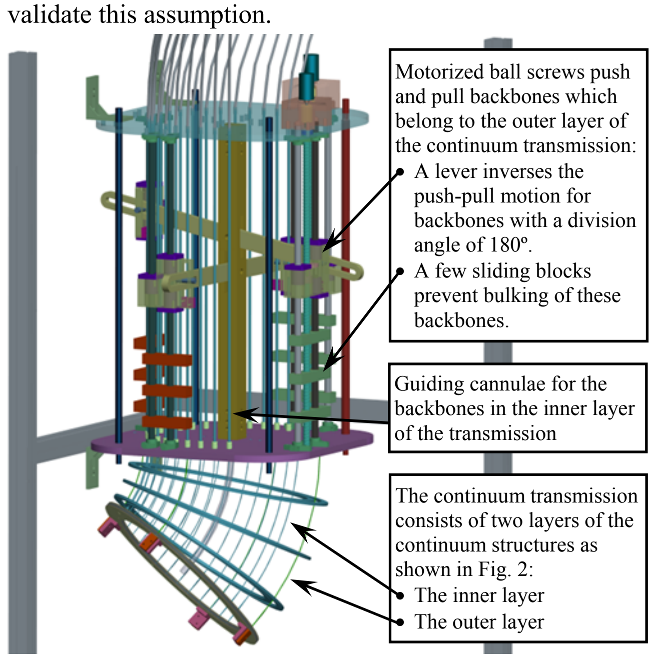

Fig. 5. The actuation unit with a continuum transmission mechanism

V. EXPERIMENTAL RESULTS

In order to demonstrate the effectiveness and advantages of the proposed continuum shoulder exoskeleton design, a series of experiments were conducted. Experimental results showed that under the same actuation and different constraints introduced by different anatomical parameters, the continuum brace adapted to the anatomies passively and deformed into different shapes. Although the deformed shapes were different, the shoulder exoskeleton managed to orient an upper arm to similar directions.

A. Shape identification of the continuum brace

The shoulder exoskeleton is shown in Fig. 6 with its actuation unit and controller. Two Maxon DC servomotors were controlled by a Matlab xPC Target to drive the ball screws according to kinematics as in Eq. (6). Motion control cards included the D/A card PCL-727 from the AdvanTech Inc and the counter card CNT32-8M from the Contec Inc.

As shown in Fig. 6.(a), three serially connected revolute joints approximate the shoulder joint since an off-the-shelf spherical joint doesn't have enough motion ranges. Axes of these revolute joints intersect at a point which is the center of the shoulder joint. Different structural components were used to introduce different distances from the shoulder joint center to the base ring of the continuum brace (the distances are 80mm, 100mm and 120mm respectively).

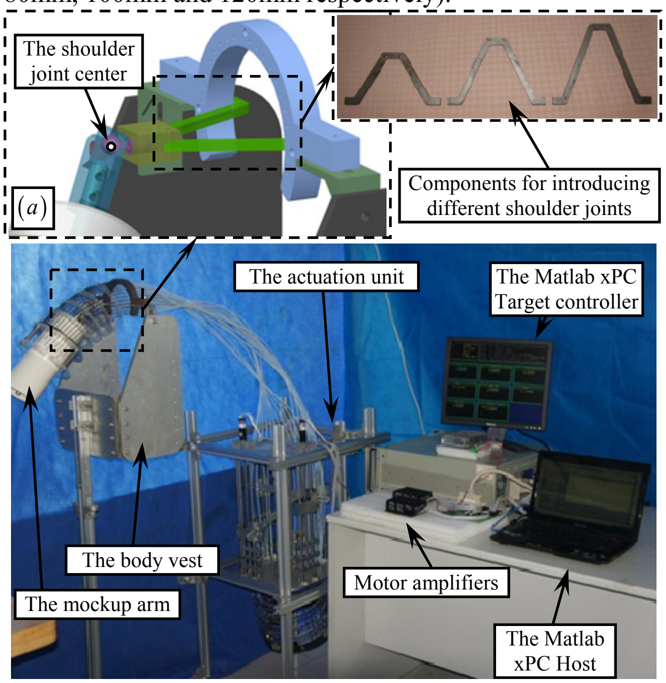

Fig. 6. The shoulder exoskeleton with its actuation unit and controller

Actuation of the continuum brace oriented the mockup arm. Pictures of the continuum brace in motion were taken to identify shapes of backbones as well as to determine bending angles of the brace. In order to minimize disturbance from gravity, the system was laid down so that the arm was sliding on a horizontal plate made from PTFE for a low friction.

The 100mm shoulder joint was used in Fig. 7 and backbone #4, #9 and #12 were picked (Numbering of the backbones is in Fig. 4). At first surrounding pixels were manually erased to expose the backbones, as shown in the inset (a). Edges were then detected and a curve was fitted to each backbone. Curve fitting results were overlaid back to the original picture to examine whether the fitted curves matched the shape of the backbones. Using the curve fitting results, a plot of bending angle versus curve length can be found in Fig. 8. According to the definition of θ_L, the bending angle is equal to $\pi/2-\theta_L$.

When a pixel is converted to an actual dimension, the conversion ratio is different for different distant object planes due to the perspective projection. In Fig. 7, two plates with a 100mm×100mm graph paper were included: one was aligned with the backbone which is closest to the camera, while the other was aligned with the backbone which is furthest to the camera. Then 100mm spanned 283 pixels for the closest plate and spanned 271 pixels for the furthest plate. Because of the 4.6% discrepancy, the length unit in Fig. 8 was kept as pixel. The unit will not affect the results of shape identification. Lens distortion was examined and found to be negligible.

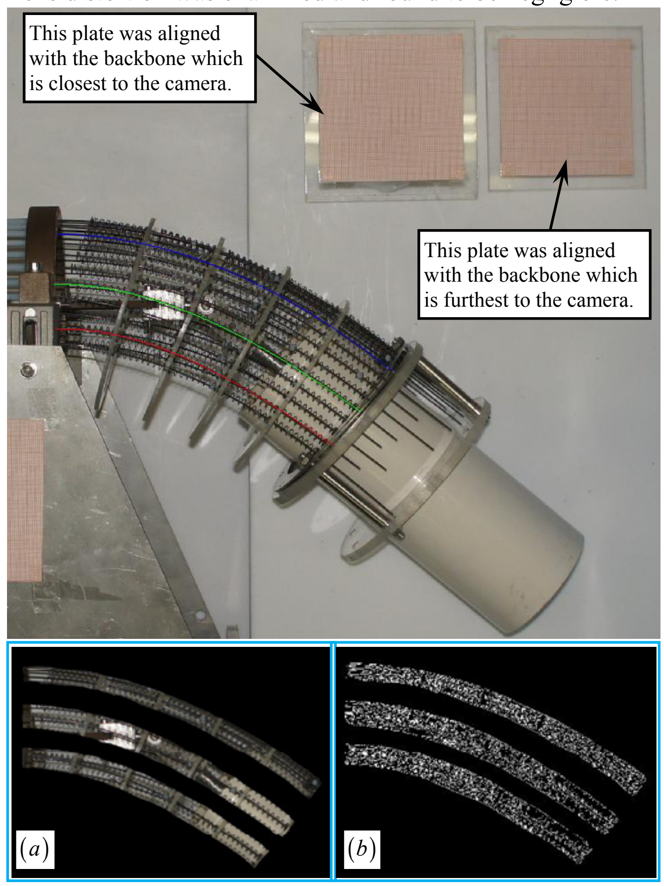

Fig. 7. Image processing & curve fitting for backbone shape identification

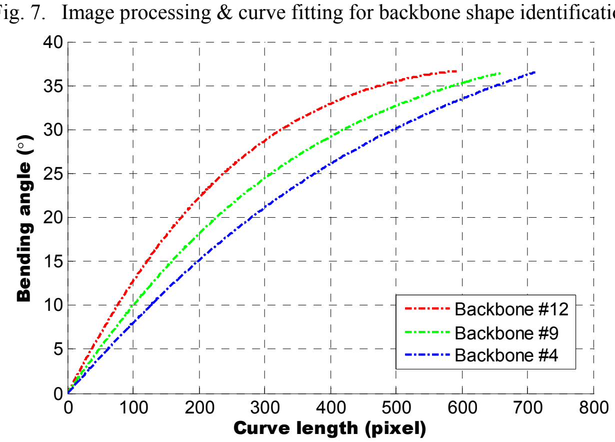

Fig. 8. Bending angles of selected backbones in the shoulder brace along their length

The two-layer continuum transmission mechanism will be deformed as in Fig 9 to drive the continuum brace. As shown in Fig. 9 and Fig. 10, shape of the backbones in both the inner and the outer layers was identified using the aforementioned process. Results from Fig. 10 indicated that backbones of the inner and the outer layers bent into similar shapes (all very close to circular arcs). The 2-layer continuum transmission bent for around 22º in Fig.10. This corresponded to the 45º bending of the shoulder brace because diameter of the inner layer is twice of the shoulder brace.

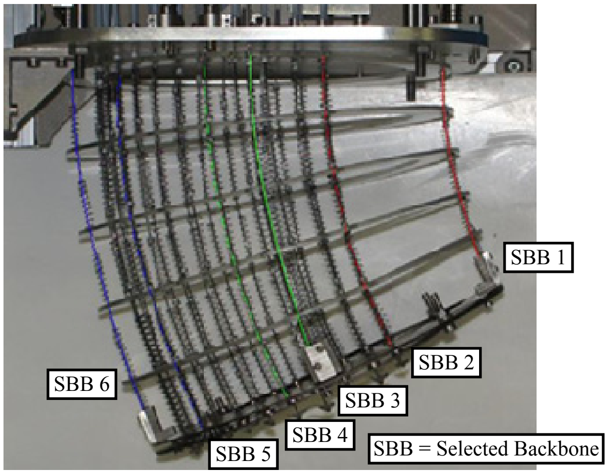

Fig. 9. Shape of selected backbones in the 2-layer continuum transmission

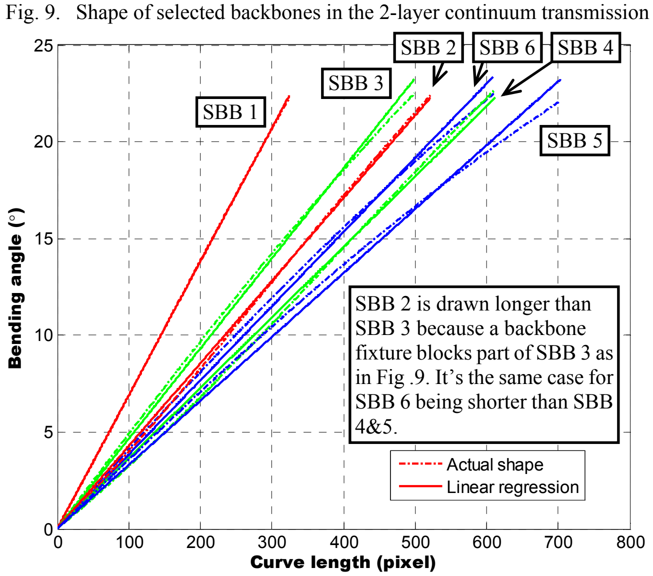

Fig. 10. Bending angles of selected backbones in the 2-layer continuum transmission mechanism along their length

The same actuation driving the continuum brace for a 100mm shoulder joint was repeated for the 80mm and the 120mm shoulder joints, and also for the case where no shoulder joint was attached. Figure 11 plots actual bending angles of the continuum brace when the desired bending angels span from 0º to 70º. The experimental data points lay closely around their linear regressions. Although bending discrepancy exists for different shoulder joints, it can be compensated using the method detailed in [40].

B. Manikin trials

The continuum shoulder exoskeleton was then put on a skeleton manikin to demonstrate the effectiveness of the proposed idea. Silicone rubber was molded to the skeleton to mimic an upper arm and rubber strips acted as the rotator cuff (including muscles and their tendons) to hold the humerus's head in its socket, as shown in Fig. 12.(a). Assisted motion of this manikin arm can be viewed in Fig 12 as well as in the multimedia extension. Because the Maxon motor used in the actuation unit only had a power rating of 6 watts with a 370:1 gearhead, the assisted motion was quite slow and the movie was speeded up.

No firm connection between the arm sleeve and the arm is needed for motion assistance. When the arm sleeve is oriented by the shoulder brace, the arm rests in the sleeve naturally, preventing the exoskeleton from exerting excessive forces on the shoulder joint.

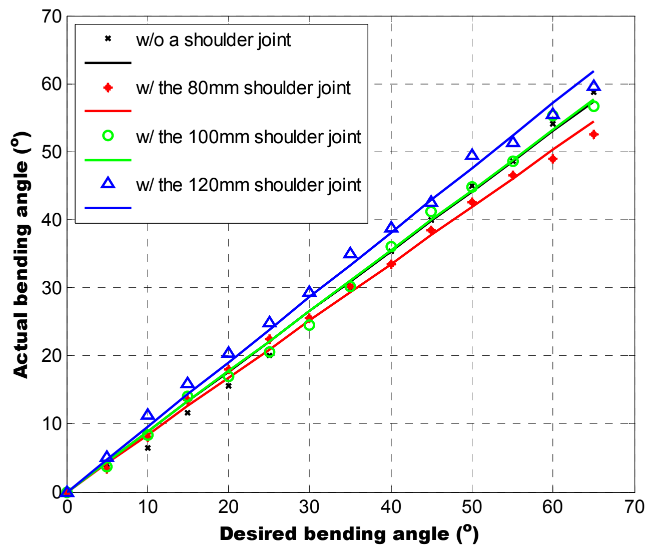

Fig. 11. Actual versus desired bending angles of the continuum brace

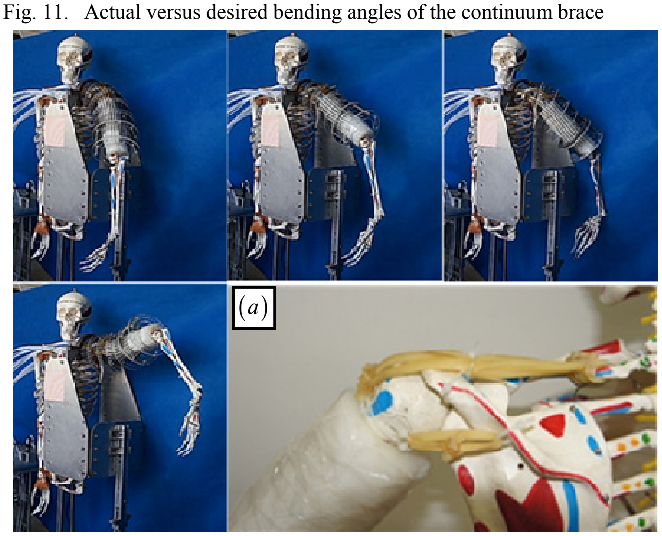

Fig. 12. Manikin trials for the continuum shoulder exoskeleton; motion pictures can be seen in the multimedia extension

VI. Conclusion and Future Work

This paper presented a novel design and its experimental verification of a continuum shoulder exoskeleton intended for rehabilitation. Backbones in the continuum brace were pushed and pulled to orient an arm sleeve and so to assist a patient with upper arm motions. During the assisted motions, the continuum exoskeleton was deformed and passively adapted to different anatomies because of its intrinsic flexibility. Although shapes of the exoskeleton were different for different anatomies, the same actuation was able to assist the anatomically different upper arms with similar motions. This is particularly advantageous for its application in a clinical setting. When the exoskeleton is shared by a group of patients, without performing any hardware adjustments, the exoskeleton can match each patient's anatomy passively and assist his/her upper arm motion. During assisted motions, no firm attachment between the arm sleeve and the arm is needed. When the arm sleeve is oriented by the shoulder brace, the arm rests in the sleeve naturally, preventing the exoskeleton from exerting excessive forces on the shoulder joint. In other words, the proposed design could potentially provide safe and effective rehabilitation to a group of anatomically different patients in an operation-friendly manner.

Future work includes deriving a more detailed kinematics model to describe the actual shape of the exoskeleton. Using this model, motion compensation could be more effectively achieved. Design ergonomics of this shoulder exoskeleton should also be further improved so that it can be used by impaired subjects. A possible solution is to design the continuum shoulder ring as two separable pieces which can be quickly assembled while putting on a patient. In this way the exoskeleton can also be conveniently peeled off when a therapeutic session is finished.

Although the current design is only for the shoulder joint, the ultimate goal is to stack more continuum braces to build a safe, light, multiple-DoF exoskeleton for the assistance of the entire upper arm.

References

[1] B. R. Brewer, S. K. McDowell, and L. C. Worthen-Chaudhari, "Poststroke Upper Extremity Rehabilitation: A Review of Robotic Systems and Clinical Results," *Topics in Stroke Rehabilitation,* vol. 14, No.6, pp. 22-44, Nov 2007.

[2] A. M. Dollar and H. Herr, "Lower Extremity Exoskeletons and Active Orthoses: Challenges and State-of-the-Art," *IEEE Transactions on Robotics,* vol. 24, No.1, pp. 144-158, Feb 2008.

[3] M. Vukobratovic, D. Hristic, and Z. Stojiljkovic, "Development of Active Anthropomorphic Exoskeletons," *Medical and Biological Engineering and Computing,* vol. 12, No.1, pp. 66-80, Jan 1974.

[4] A. B. Zoss, H. Kazerooni, and A. Chu, "Biomechanical Design of the Berkeley Extremity Exoskeleton (BLEEX)," *IEEE/ASME Transaction on Mechatronics,* vol. 11, No.2, pp. 128-138, April 2006.

[5] C. J. Walsh, D. Paluska, K. Pasch, W. Grand, A. Valiente, and H. Herr, "Development of a Lightweight, Underactuated Exoskeleton for Load-Carrying Augmentation," in *IEEE International Conference on Robotics and Automation (ICRA)*, Orlando, Florida, USA, 2006.

[6] W. K. Durfee and A. Rivard, "Priliminary Design and Simulation of a Pneumatic, Stored-Energy, Hybrid Orthosis for Gait Restoration," in *ASME International Mechanical Engineering Congress*, Anaheim, California USA, 2004, pp. 1-7.

[7] S. K. Banala, S. K. Agrawal, A. Fattah, V. Krishnamoorthy, W.-L. Hsu, J. Scholz, and K. Rudolph, "Gravity-Balancing Leg Orthosis and Its Performance Evaluation," *IEEE Transactions on Robotics,* vol. 22, No.6, pp. 1228-1239, 2006.

[8] J. F. Veneman, R. Ekkelenkamp, R. Kruidhof, F. C. T. van der Helm, and H. van der Kooij, "A Series Elastic- and Bowden-Cable-Based Actuation System for Use as Torque Actuator in Exoskeleton-Type Robots," *International Journal of Robotics Research,* vol. 25, No.3, pp. 261-281, March 2006.

[9] J. A. Saglia, N. G. Tsagarakis, J. S. Dai, and D. G. Caldwell, "A High Performance 2-dof Over-Actuated Parallel Mechanism for Ankle Rehabilitation," in *IEEE International Conference on Robotics and Automation (ICRA)*, Kobe, Japan, 2009, pp. 2180-2186.

[10] R. J. Farris, H. A. Quintero, and M. Goldfarb, "Preliminary Evaluation of a Powered Lower Limb Orthosis to Aid Walking in Paraplegic Individuals," *IEEE Transactions on Neural Systems and Rehabilitation Engineering,* vol. 19, No.6, pp. 652-659, Dec 2011.

[11] N. G. Tsagarakis and D. G. Caldwell, "Development and Control of a 'Soft-Actuated' Exoskeleton for Use in Physiotherapy and Training," *Autonomous Robots,* vol. 15, No.1, pp. 21-33, 2003.

[12] J. C. Perry, J. Rosen, and S. Burns, "Upper-Limb Powered Exoskeleton Design," *IEEE/ASME Transaction on Mechatronics,* vol. 12, No.4, pp. 408-417, Aug 2007.

[13] A. Gupta, M. K. O'Malley, V. Patoglu, and C. Burgar, "Design, Control and Performance of RiceWrist: A Force Feedback Wrist Exoskeleton for Rehabilitation and Training," *International Journal of Robotics Research,* vol. 27, No.2, pp. 233-251, Feb 2008.

[14] A. H. A. Stienen, E. E. G. Hekman, G. B. Prange, M. J. A. Jannink, A. M. M. Aalsma, F. C. T. v. d. Helm, and H. v. d. Kooij, "Dampace: Design of an Exoskeleton for Force-Coordination Training in Upper-Extremity Rehabilitation," *Journal of Medical Devices,* vol. 3, No.031003, pp. 1-10, Sept 2009.

[15] J. Klein, S. Spencer, J. Allington, J. E. Bobrow, and D. J. Reinkensmeyer, "Optimization of a Parallel Shoulder Mechanism to Achieve a High-Force, Low-Mass, Robotic-Arm Exoskeleton," *IEEE Transactions on Robotics,* vol. 26, No.4, pp. 710-715, Aug 2010.

[16] E. T. Wolbrecht, D. J. Reinkensmeyer, and J. E. Bobrow, "Pneumatic Control of Robots for Rehabilitation," *International Journal of Robotics Research,* vol. 29, No.1, pp. 23-38, Jan 2010.

[17] S. K. Agrawal, V. N. Dubey, J. J. Gangloff, E. Brackbill, Y. Mao, and V. Sangwan, "Design and Optimization of a Cable Driven Upper Arm Exoskeleton," *Journal of Medical Devices,* vol. 3, No.031004, pp. 1-8, Sept 2009.

[18] Y. Mao and S. K. Agrawal, "Design of a Cable-Driven Arm Exoskeleton (CAREX) for Neural Rehabilitation," *IEEE Transactions on Robotics,* vol. 28, No.4, pp. 922-931, Aug 2012.

[19] R. C. V. Loureiro and W. S. Harwin, "Reach & Grasp Therapy: Design and Control of a 9-DOF Robotic Neuro-rehabilitation System," in *IEEE International Conference on Rehabilitation Robotics (ICORR)*, Noordwijk, The Netherlands, 2007, pp. 757-763.

[20] G. Aguirre-Ollinger, J. E. Colgate, M. A. Peshkin, and A. Goswami, "Design of an Active One-Degree-of-Freedom Lower-Limb Exoskeleton with Inertia Compensation," *International Journal of Robotics Research,* vol. onlinefirst, Dec 2010.

[21] H. Kawamoto, S. Lee, S. Kanbe, and Y. Sankai, "Power Assist Method for HAL-3 using EMG-based Feedback Controller," in *IEEE International Conference on Systems, Man and Cybernetics (IEEE SMC)*, Washington, D.C., USA, 2003, pp. 1648-1653.

[22] K. Yamamoto, M. Ishii, H. Noborisaka, and K. Hyodo, "Stand Alone Wearable Power Assisting Suit: Sensing and Control Systems," in *IEEE International Workshop on Robot and Human Interactive Communication*, Kurashiki, Okayama, Japan, 2004.
[23] C. Fleischer and G. Hommel, "A Human–Exoskeleton Interface Utilizing Electromyography," *IEEE Transactions on Robotics,* vol. 24, No.4, pp. 872-882, Aug 2008.
[24] V. Sharma, D. B. McCreery, M. Han, and V. Pikov, "Bidirectional Telemetry Controller for Neuroprosthetic Devices," *IEEE Transactions on Neural Systems and Rehabilitation Engineering,* vol. 18, No.1, pp. 67-74, Feb 2010.
[25] A. Schiele and F. C. T. van der Helm, "Kinematic Design to Improve Ergonomics in Human Machine Interaction," *IEEE Transactions on Neural Systems and Rehabilitation Engineering,* vol. 14, No.4, pp. 456-469, Dec 2006.
[26] H. Kim, L. M. Miller, N. Byl, G. M. Abrams, and J. Rosen, "Redundancy Resolution of the Human Arm and an Upper Limb Exoskeleton," *IEEE Transactions on Biomedical Engineering,* vol. 59, No.6, pp. 1770-1779, June 2012.
[27] N. Jarrassé and G. Morel, "Connecting a Human Limb to an Exoskeleton," *IEEE Transactions on Robotics,* vol. 28, No.3, pp. 697-709, June 2012.
[28] A. H. A. Stienen, E. E. G. Hekman, H. t. Braak, A. M. M. Aalsma, F. C. T. v. d. Helm, and H. v. d. Kooij, "Design of a Rotational Hydroelastic Actuator for a Powered Exoskeleton for Upper Limb Rehabilitation," *IEEE Transactions on Biomedical Engineering,* vol. 57, No.3, pp. 728-735, March 2010.
[29] M. Bergamasco, F. Salsedo, S. Marcheschi, N. Lucchesi, and M. Fontana, "A Novel Compact and Lightweight Actuator for Wearable Robots," in *IEEE International Conference on Robotics and Automation (ICRA)*, Anchorage, Alaska, USA, 2010, pp. 4197-4203.
[30] A. J. van den Bogert, "Exotendons for assistance of human locomotion," *Biomedical Engineering Online,* vol. 2, No.17, Oct 2003.
[31] H. Kobayashi and K. Hiramatsu, "Development of Muscle Suit for Upper Limb," in *IEEE International Conference on Robotics and Automation (ICRA)*, New Orleans, LA, USA, 2004, pp. 2480-2485.
[32] K. Xu, D. Qiu, and N. Simaan, "A Pilot Investigation of Continuum Robots as a Design Alternative for Upper Extremity Exoskeletons," in *IEEE International Conference on Robotics and Biomimetics (ROBIO)*, Phuket, Thailand, 2011, pp. 656-662.
[33] K. Xu, R. E. Goldman, J. Ding, P. K. Allen, D. L. Fowler, and N. Simaan, "System Design of an Insertable Robotic Effector Platform for Single Port Access (SPA) Surgery," in *IEEE/RSJ International Conference on Intelligent Robots and Systems (IROS)*, St. Louis, MO, USA, 2009, pp. 5546-5552.
[34] N. Simaan, K. Xu, A. Kapoor, W. Wei, P. Kazanzides, P. Flint, and R. H. Taylor, "Design and Integration of a Telerobotic System for Minimally Invasive Surgery of the Throat " *International Journal of Robotics Research,* vol. 28, No.9, pp. 1134-1153, 2009.
[35] K. Xu and N. Simaan, "Analytic Formulation for the Kinematics, Statics and Shape Restoration of Multibackbone Continuum Robots via Elliptic Integrals," *Journal of Mechanisms and Robotics,* vol. 2, Feb 2010.
[36] K. Xu and N. Simaan, "An Investigation of the Intrinsic Force Sensing Capabilities of Continuum Robots," *IEEE Transactions on Robotics,* vol. 24, No.3, pp. 576-587, June 2008.
[37] K. Xu and N. Simaan, "Intrinsic Wrench Estimation and Its Performance Index of Multi-Segment Continuum Robots," *IEEE Transactions on Robotics,* vol. 26, No.3, pp. 555-561, June 2010.
[38] R. J. Webster and B. A. Jones, "Design and Kinematic Modeling of Constant Curvature Continuum Robots: A Review " *International Journal of Robotics Research,* vol. 29, No.13, pp. 1661-1683, Nov 2010.
[39] J. Rosen, J. C. Perry, N. Manning, S. Burns, and B. Hannaford, "The Human Arm Kinematics and Dynamics during Daily Activities - toward a 7 DOF Upper Limb Powered Exoskeleton," in *IEEE International Conference on Advanced Robotics (ICAR)*, Seattle, WA, 2005, pp. 532-539.
[40] K. Xu and N. Simaan, "Actuation Compensation for Flexible Surgical Snake-like Robots with Redundant Remote Actuation," in *IEEE International Conference on Robotics and Automation (ICRA)*, Orlando, Florida, USA, 2006, pp. 4148-4154.